 Related Commentary, page 886

Dysregulation of insulin receptor substrate 2 in β cells and brain causes obesity and diabetes

Xueying Lin, Akiko Taguchi, Sunmin Park, Jake A. Kushner, Fan Li, Yedan Li, and Morris F. White

Howard Hughes Medical Institute Children's Hospital, Division of Endocrinology, Harvard Medical School, Boston, Massachusetts, USA.

The molecular link between obesity and β cell failure that causes diabetes is difficult to establish. Here we show that a conditional knockout of insulin receptor substrate 2 (Irs2) in mouse pancreas β cells and parts of the brain — including the hypothalamus —increased appetite, lean and fat body mass, linear growth, and insulin resistance that progressed to diabetes. Diabetes resolved when the mice were between 6 and 10 months of age: functional β cells expressing Irs2 repopulated the pancreas, restoring sufficient β cell function to compensate for insulin resistance in the obese mice. Thus, Irs2 signaling promotes regeneration of adult β cells and central control of nutrient homeostasis, which can prevent obesity and diabetes in mice.

Introduction

Type 2 diabetes affects 18.2 million people in the United States and is increasingly common among young people (1, 2). Most disease models point to obesity as an important cause of type 2 diabetes, because of its association with skeletal muscle insulin resistance and pancreatic β cell failure (3, 4). However, dysregulated peripheral and central signaling — owing to many different causes — might initiate and sustain the cascade of events that progress to obesity and diabetes. Most if not all insulin signals are produced or modulated through tyrosine phosphorylation of insulin receptor substrate 1 (IRS1); IRS2 or its homologs; or other scaffold proteins including Src-homology-2 (SH2) domains including SH2 domain containing Shc, Casitas B-lineage lymphoma proto-oncogene (c-CBL), adapter protein with a PH and SH2 domain (APS) and SH2 and PH domain containing signaling mediator 1 (SH2B), Grb-2 associated binder-I (GAB1), GAB2, or dreadlocks (DOCK, an SH3-SH2 adaptor protein) isoforms (5). Although the role of each of these substrates merits attention, cell-based experiments and work with transgenic mice suggest that many insulin responses are directly integrated with counterregulatory hormones and proinflammatory cytokines through tyrosine and serine phosphorylation of IRS1 and IRS2 (5). Dysregulation of these IRS proteins by proinflammatory cytokines or genetic deletion impairs glucose tolerance as a result of peripheral insulin resistance; however, systemic *Irs2*$^{-/-}$ mice also develop life-threatening diabetes at 2–3 months of age because Irs2 is required for β cell growth, function, and survival (6–9). The progression of *Irs2*$^{-/-}$ mice toward diabetes is retarded or prevented by modifying elements of the insulin/IGF-signaling cascade that promote compensatory β cell function — including downregulation of protein tyrosine phosphatase Ptp1b or the transcription factor Foxo1; or upregulation of Akt (also called protein kinase B, or PKB) or pancreatic duodenal homeobox 1 (Pdx1) (9–14). Transgenic upregulation of Irs2 in pancreatic β cells also prevents diabetes in *Irs2*$^{-/-}$ mice, obese mice, and streptozotocin-induced diabetic mice by promoting sufficient and sustained compensatory insulin secretion (9). Thus, the Irs2 branch of the insulin/IGF-signaling cascade is a common link between peripheral insulin action and secretion.

A molecular basis for the close association between obesity and peripheral insulin resistance is difficult to establish. Dysregulated signaling — rather than antidotal consumption of high-calorie diets — might contribute to the early development of obesity that progresses to diabetes (15–17). Insulin, leptin, and adiponectin are important peripheral signals that inform the brain of short- and long-term nutrient availability (17–19). Pharmacologic inhibition of insulin signaling in the hypothalamus increases food intake, and conditional KO of the insulin receptor in the brain causes obesity in mice on high-fat diets (20–23). Leptin secreted from adipocytes promotes satiety and energy utilization, at least in part by promoting α melanocyte–stimulating hormone (αMSH) production in the hypothalamus (15). Mutations that disrupt neuronal leptin signaling or melanocortin signaling increase food intake, body weight, and peripheral insulin resistance in mice and people that progresses to diabetes if β cell function also deteriorates (24–26). Adiponectin, another adipocyte-derived hormone, enhances hepatic and muscle insulin action and promotes energy expenditure through signaling in the hypothalamus (18, 27); however, adiponectin is reduced in obese people and rodents (28, 29).

Previous work suggests that Irs2 signaling plays an important role in the CNS for brain growth, female fertility, and nutrient homeostasis (30). Since IRS2 is highly expressed in the hypothalamus, its signaling cascade may be responsible for integrating central control of nutrient homeostasis and appetite regulation with peripheral insulin action and β cell function (9). Female *Irs2*$^{-/-}$ mice — which develop diabetes more slowly than do male mice — are hyperphagic and obese until severe diabetes causes weight loss (30). To test the role of selective Irs2 dysregulation in obesity and diabetes, we flanked the *Irs2* gene with *loxP* recombination sites (floxed *Irs2*, or *fIrs2*) and crossed these mice with transgenic mice expressing Cre recombinase under control of the rat insulin-2 promoter (TgN[Ins2Cre]25Mgn mice, or *cr*^{2} mice). Cre recombinase is expressed strongly in β cells and weakly in certain brain regions of these transgenic *cr*^{2} mice (31, 32). Thus, our strategy strongly deleted *fIrs2* alleles from β cells and weakly deleted them from brain and

Nonstandard abbreviations used: *cr*^{2}, TgN[Ins2Cre]25Mgn; *fIrs2*, floxed *Irs2*; GLP1, glucagon-like peptide 1; Irs, insulin receptor substrate; Mc4r, melanocortin 4 receptor; αMSH, α melanocyte–stimulating hormone; Pdx1, pancreatic duodenal homeobox 1; Pomc, pro-opiomelanocortin; Stat3, signal transducer and activator of transcription 3.

Conflict of interest: The authors have declared that no conflict of interest exists.

Citation for this article: *J. Clin. Invest.* **114**:908–916 (2004). doi:10.1172/JCI200422217.

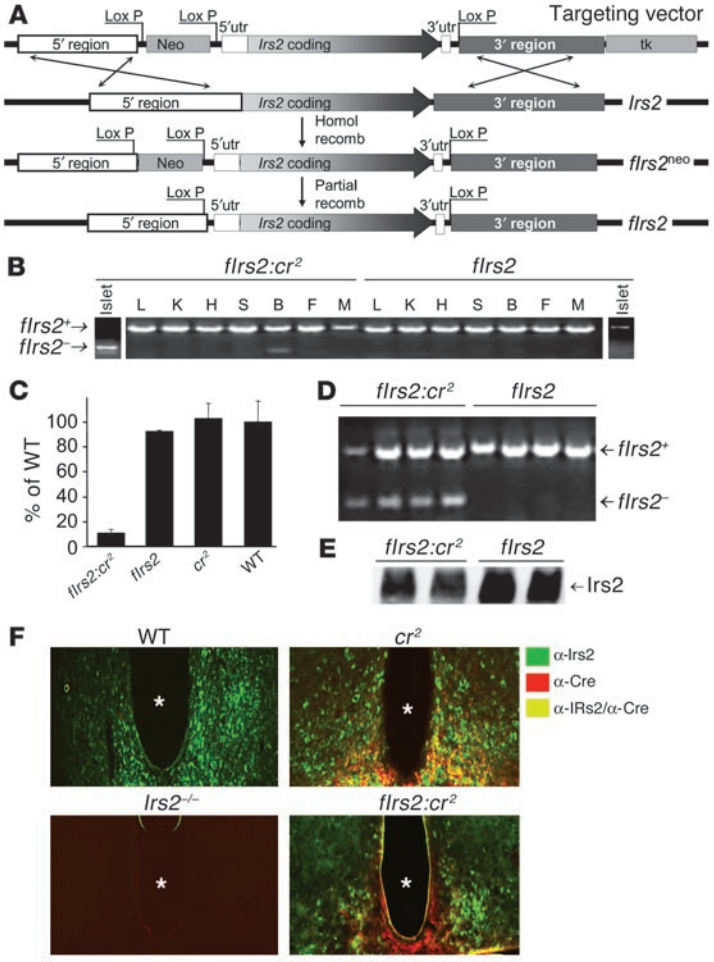

Figure 1
Creation of *flrs2* mice and *cr²*-mediated recombination/deletion of *flrs2*. (**A**) A schematic diagram of the 4 steps in the generation of the *flrs2* containing embryonic stem cells (see Methods for details). Homol recomb, homologous recombination. (**B**) Recombination/deletion of *flrs2* was revealed in various mouse tissues at 4 weeks of age by PCR analysis of genomic DNA. L, liver; K, kidney; H, heart; S, spleen; B, brain, F, fat; M, muscle. The intact *flrs2* allele (*flrs2*⁺) yields a 750-bp fragment, whereas the recombined/deleted allele (*flrs2*⁻) yields a 250-bp fragment. (**C**) Real-time PCR analysis of *Irs2* expression in isolated islets, normalized by *cyclophilin* expression. (**D**) PCR analysis of hypothalamic DNA to reveal recombination event. (**E**) Immunoprecipitation and Western blot analysis of hypothalamus with antibodies against Irs2. (**F**) Brain sections were immunostained with antibodies against Irs2 (red) and Cre (green), and the images were merged in Openlab Image software (version 3.14; Improvision). Similar results were obtained with multiple sections from 2 to 8 mice. Asterisks indicate third ventricle. Magnification, ×20.

certain neurons of the hypothalamus. Analysis of the mice suggests that dysregulated Irs2 signaling could be a common link between obesity and β cell failure that progresses to diabetes; and that Irs2 signaling is an important element for β cell regeneration.

Results

Conditional disruption of floxed Irs2 allele by cr². To determine whether partial dysregulation of Irs2 signaling links obesity and diabetes, we intercrossed mice containing homozygous *flrs2* alleles with *cr²* mice (Figure 1A). PCR analysis of islets from the compound *flrs2:cr²* mice (4 weeks old) confirmed that *flrs2* alleles were almost completely deleted, which was consistent with the reported efficacy of *cr²* in β cells (Figure 1B). Since islets are composed mainly of β cells, *Irs2* mRNA levels decreased at least 90% (Figure 1C). *flrs2* alleles were partially deleted in the brain, including regions of the hypothalamus (Figure 1, B and D), which is consistent with the reported expression of *cr²* in some neurons (31, 32). At 8 weeks, Irs2 protein levels were reduced at least 30% in *flrs2:cr²* hypothalamic extracts (Figure 1E). By contrast, *flrs2* was intact and protein levels were normal in other tested tissues, including muscle, liver, and fat (Figure 1B and data not shown).

To verify that *flrs2* was disrupted in hypothalamic neurons, we immunostained sections of the arcuate nucleus with antibodies against Irs2 (green stain) and Cre recombinase (red stain); low background was confirmed in systemic *Irs2*⁻/⁻ brain sections that lack both proteins (Figure 1F). Irs2 was detected in the arcuate nucleus from WT or *cr²* mice, and Cre recombinase was detected in *cr²* mice, where it was expressed in some (yellow staining) but not all Irs2-positive neurons (Figure 1F). However, coexpression of Irs2 and Cre was largely abolished in *flrs2:cr²* sections, which confirmed that *flrs2* was deleted wherever Cre was expressed (Figure 1F); similar results were found in paraventricular nucleus (data not shown).

Growth of the flrs2:cr² mice. The *flrs2:cr²* mice reached a normal body weight at 4 weeks of age but then grew more rapidly and were 30% heavier than controls when the experiment was terminated at 32 weeks (Figure 2A). At 8 weeks, *flrs2:cr²* mice were 8 grams heavier than the controls (*flrs2:cr²*, 38.2 ± 0.6 g, $P < 0.01$ compared with *flrs2*, 29.8 ± 0.5 g; *cr²*, 29.4 ± 0.8 g; and WT, 29.1 ± 0.6 g); and they consumed 60% ($P < 0.05$) more chow (9% fat) and 65% ($P = 0.001$) more water than did the control mice during a 24-hour interval (Figure 2, B and C). Unlike systemic *Irs2*⁻/⁻ mice, which have small brains (33), the *flrs2:cr²* mice had a normal brain size (*flrs2:cr²*, 0.41 ± 0.01 g; *flrs2*, 0.40 ± 0.01 g; *cr²*, 0.40 ± 0.02 g; and WT, 0.40 ± 0.02 g).

The *flrs2:cr²* mice were 10% longer — snout to anus — than the controls (*flrs2:cr²*, 107.9 ± 0.5 mm, $P < 0.01$ compared with *flrs2*, 98 ± 2 mm; *cr²*, 96.5 ± 0.4 mm; WT, 98 ± 1 mm). On the normal 9% fat diet, 8-week-old *flrs2:cr²* mice had 2-fold more body fat and increased lean body mass (Figure 2D). Chemical analysis confirmed that fat mass was increased disproportionately in *flrs2:cr²* mice (*flrs2:cr²*, 18% ± 3% fat, $n = 5$; *flrs2*, 11% ± 1% fat, $n = 4$; $P = 0.005$). Consistent with the increased adiposity, serum leptin and insulin levels were elevated 2-fold in the *flrs2:cr²* mice compared with controls (Figure 2E). Because of their larger size, *flrs2:cr²* mice produced more heat than control mice during a 24-hour period (*flrs2:cr²*, 14.1 ± 0.1 kcal; WT, 11.0 ± 1.5 kcal). Although caloric restriction achieved by feeding the mice a low-fat (5%) diet reduced the weight of all the mice, the *flrs2:cr²* mice were consistently heavier (Figure 2A).

Glucose homeostasis in the flrs2:cr² mice. Diabetes developed in the *flrs2:cr²* mice between 8 and 10 weeks of age, as fasting glucose levels exceeded those of the control mice (*flrs2:cr²*, 110 ± 9 mg/dl, $P < 0.01$ compared with *flrs2*, 63 ± 2 mg/dl; *cr²*, 60 ± 4 mg/dl; WT, 62 ± 6 mg/dl). Moreover, random-fed glucose was consistently 2-fold higher in the *flrs2:cr²* mice than in the controls (Figure 2A). Glucose disposal rates measured in the *flrs2:cr²* mice — during a hyperinsulinemic/

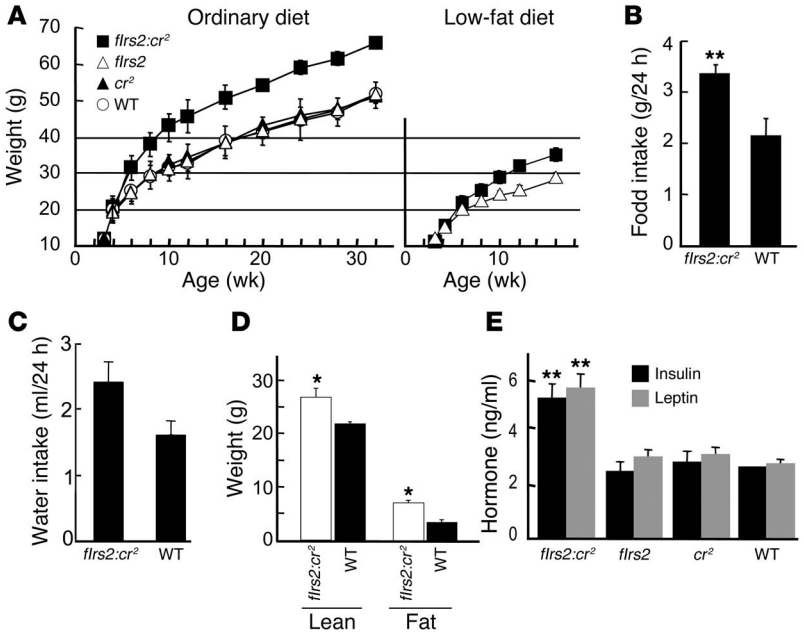

Figure 2
Growth and nutrient homeostasis of the *flrs2:cr²* mice. (**A**) Male littermates fed regular or low-fat chow were weighed weekly from postnatal day 21 until 32 weeks of age; each point represents the average ± SE of at least 6 mice. Omitted error bars are smaller than the symbol. (**B**) Food intake was determined with 8-week-old male mice over 24 hours using a Comprehensive Lab Animal Monitoring System; average ± SE for 4 animals per genotype is reported. (**C**) Cumulative water intake was determined with 8-week-old male mice over 24 hours using a Comprehensive Lab Animal Monitoring System; average ± SE for 3 animals per genotype is reported. (**D**) Average lean and fat body mass ± SE was determined on three 8-week-old male of the indicated genotypes using a dual energy X-ray absorptiometry (DEXA) scanner (GE Medical Systems Lunar) according to the manufacturer's instructions. (**E**) Average ± SE plasma insulin and leptin levels were determined on at least fifteen 8-week-old random fed male mice of each genotype using a rat insulin or mouse leptin ELISA Kit. **P* < 0.05; ***P* < 0.01.

euglycemic clamp test — were reduced 50%, which revealed peripheral insulin resistance, an important hallmark of type 2 diabetes (Figure 2B). By contrast, hepatic glucose output measured before and during experimental hyperinsulinemia was similar in all of the mice examined (Figure 3C).

The insulin content of the *flrs2:cr²* pancreas was reduced more than 2-fold compared with that in the control mice (Figure 3D). This result is consistent with a positive role for IRS2 in β cell function, especially during compensation for peripheral insulin resistance (9). Intraperitoneal glucose injections following a 16-hour overnight fast confirmed glucose intolerance and diabetes in *flrs2:cr²* mice (Figure 3E). Although glucose tolerance improved when the *flrs2:cr²* mice were placed on the low-fat diet, *flrs2:cr²* mice remained hyperinsulinemic (*flrs2:cr²*, 2.5 ± 0.2 ng/ml, $P < 0.01$ compared with *flrs2*, 0.7 ± 0.1 ng/ml; *cr²*, 0.6 ± 0.1 ng/ml; WT, 0.5 ± 0.1 ng/ml) and relatively glucose intolerant in comparison with control mice on the low-fat diet (Figure 3F).

β cell growth and function in flrs2:cr² mice. The growth, function, and survival of β cells are essential for normal glucose homeostasis, especially during compensation for peripheral insulin resistance. At 4 weeks of age when the *flrs2:cr²* mice had a normal body weight, relative β cell content — estimated by the average β cell area in pancreas sections — and β cell size were indistinguishable from those of control mice (Table 1). The expression of several genes that promote β cell function and growth — *hepatocyte nuclear factor 3* β (*Hnf3*β), *Hnf4*α, and *Pdx1* — were decreased in *flrs2:cr²* islets; however, *glucose transporter 2* (*Glut2*) mRNA levels were nearly normal

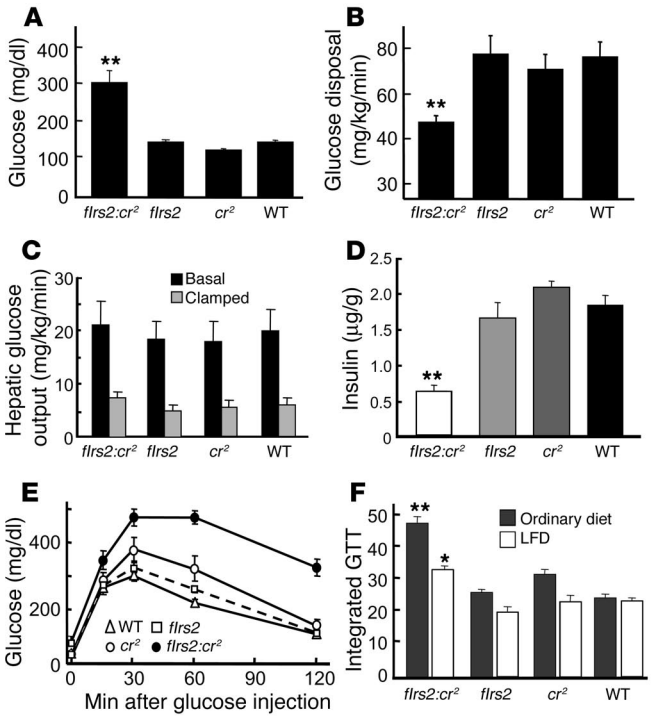

Figure 3
Glucose homeostasis in the *flrs2:cr²* mice. (**A**) Average ± SE random-fed blood glucose levels were determined using a Glucometer Elite in at least fifteen 8-week-old male mice of the indicated genotypes. (**B** and **C**) Glucose-disposal rates and hepatic glucose output before and during hyperinsulinemia (average ± SE) were determined on 6–10 fasted and conscious 10-week-old male mice of the indicated genotypes. (**D**) Pancreas insulin content was determined using rat insulin ELISA Kit following acid-ethanol extraction. Results are average ± SE for five 8-week-old mice per genotype. (**E**) After a 16-hour overnight fast, blood glucose (average ± SE) was determined on at least fifteen 8-week-old male mice of the indicated genotypes following intraperitoneal injection of 2 g D-glucose/kg body weight. (**F**) The integrated glucose tolerance (GTT, t = 0 → 120 min) for the 8-week old male mice fed the ordinary diet (data in **E**) was compared with that for 16-week-old male mice fed a low-fat diet (LFD, 5%); these ages were selected for comparison to match the body weights. The glucose tolerance curves were integrated using the trapezoid rule implemented in Sigmaplot 8.0 (Systat Software Inc.). **P* < 0.05; ***P* < 0.01.

Table 1
Islet characteristics

	fIrs2:cr²	*fIrs2:cr²:Irs1⁺/⁻*	*fIrs2*	*fIrs2:Irs1⁺/⁻*	*cr²*	WT
4 weeks						
β Cell area	0.5 ± 0.1(4)	–	–	–	–	0.5 ± 0.1 (5)
β Cell size	77± 8 (4)	–	75 ± 6 (6)	–	86 ± 10 (3)	78 ± 7 (5)
BrdU (%)	2.0 ± 0.4 (4)	–	1.5 ± 0.2 (6)	–	1.1 ± 0.2 (3)	1.6 ± 0.3 (5)
Real-time PCR						
*Hnf3*β (%)	41 ± 7 (4)[A]	–	98 ± 11 (5)	–	94 ± 15 (4)	100 ± 8 (4)
Pdx1(%)	46 ± 4 (4)[B]	–	103 ± 9 (5)	–	107 ± 1 (4)	100 ± 7 (4)
*Hnf4*α (%)	30 ± 1 (4)[A]	–	99 ± 13 (5)	–	89 ± 23 (4)	100 ± 11 (4)
Glut2 (%)	69 ± 12 (4)	–	93 ± 10 (5)	–	97 ± 15 (4)	100 ± 8 (4)
8 weeks						
β Cell area	0.45 ± 0.06 (5)[A]	–	0.94 ± 0.08 (6)	–	0.9 ± 0.1(4)	0.88 ± 0.07 (5)
6 months						
β Cell area	1.1 ± 0.1 (5)	0.20 ± 0.05 (6)	–	1.6 ± 0.2 (6)	–	1.1 ± 0.1 (5)
10 months						
β Cell area (% of total)	3.4 ± 0.1 (5)	–	3.5 ± 0.6(4)	–	3.7 ± 0.1 (4)	3.3 ± 0.5 (4)
β Cell mass (μg/pancreas)	1,698 ± 79 (5)	–	1414 ± 246 (4)	–	1341 ± 91 (4)	1,389 ± 248 (4)
Islets/pancreas (<10 β cells)	52 ± 9 (4)[A]	–	–	–	–	30 ± 6 (3)
Islets/pancreas (<10 β cells)	25 ± 6 (4)[A]	–	–	–	–	22 ± 3 (3)
Total islets/pancreas	77 ± 11	–	–	–	–	52 ± 7

Islet characteristics were calculated as previously described (9) and summarized briefly in Methods. The number of animals used for each genotype and the average ± SE is reported. [A]$P < 0.05$; [B]$P < 0.01$. –, not determined.

(Table 1). DNA synthesis — estimated by in situ BrdU incorporation—was not significantly different in *fIrs2:cr²* islets (Table 1). Nevertheless, β cell content in the *fIrs2:cr²* mice did not increase during the next 4 weeks, contrary to what was observed in 8-week-old control mice. These characteristics were consistent with the reduced insulin content of the *fIrs2:cr²* pancreas (Figure 3D).

Based upon our experience with systemic *Irs2*$^{-/-}$ mice (9), we expected hyperglycemia to progress and eventually kill the *fIrs2:cr²* mice; however, diabetes always resolved spontaneously between 6 and 8 months of age (Figure 4A). At 6 months, relative β cell content of *fIrs2:cr²* mice was normal in comparison with WT mice; and by 10 months, the relative β cell mass increased in all of the mice to compensate for peripheral insulin resistance that always emerges as the mice age and gain weight (Table 1). The nondiabetic *fIrs2:cr²* mice remained heavier than the control mice (*fIrs2:cr²*, 68 ± 2 g; *fIrs2*, 51 ± 2 g; *cr²*, 53 ± 1 g); and owing to a larger pancreas at 10 months, the total β cell mass in *fIrs2:cr²* mice was slightly greater than that in controls (Table 1). At 10 months, pancreas sections from *fIrs2:cr²* mice contained more islets, but a disproportionate number of the islet sections contained fewer than 10 β cells (Table 1). Thus, persistent insulin resistance was balanced by the growth of functional β cells that maintained compensatory hyperinsulinemia in mice at 10 months of age (Figure 4B); and during the next year, these mice did not develop diabetes.

What reversed the progression to diabetes? We isolated individual islets from *fIrs2:cr²* mice at 4, 6, and 10 months of age and used PCR to identify the presence or absence of the *fIrs2* allele. At 4 months, most islets lacked *fIrs2*, whereas a few islets displayed a mixture of deleted and intact *fIrs2* (Figure 4C). At 6 months, islets contained either deleted *fIrs2*, intact *fIrs2*, or a mixture of these alleles; and by 10 months, deleted *fIrs2* was never detected (Figure 4C). Thus, *fIrs2*$^{-/-}$ β cells were progressively replaced by β cells containing *fIrs2*. The progressive decline of Cre recombinase in islets between 1 and 12 months of age suggests that regenerated β cells arise from cells that weakly express Cre recombinase (Figure 4D); however, we cannot establish the source of these new β cells.

The role of IRS1 in β cell regeneration. Peripheral insulin action is mediated by both Irs1 and Irs2 (5); however, systemic *Irs1*$^{-/-}$ mice never develop diabetes, as Irs2 promotes β cell growth and function to compensate for peripheral insulin resistance (34). Previous work shows that *Irs1* haploinsufficiency strongly inhibits residual growth, function, and survival of β cells in systemic *Irs2*$^{-/-}$ mice, as β cells are nearly undetected when systemic *Irs2*$^{-/-}$*:Irs1*$^{+/-}$ mice die at 30 days of age (34). To determine whether Irs1 contributes to the regeneration of β cells in *fIrs2:cr²* mice, we intercrossed *fIrs2:cr²* mice with systemic *Irs1*$^{+/-}$ mice to produce compound *[fIrs2:cr²]:Irs1*$^{+/-}$ mice. Unlike systemic *Irs1*$^{+/-}$ mice or *fIrs2:cr²* mice, the *[fIrs2:cr²]:Irs1*$^{+/-}$ mice developed diabetes at 4 weeks (Figure 4A). The early-onset diabetes progressed rapidly to severe hyperglycemia as serum insulin levels fell during the next several months (Figure 4B). As a result of progressive and severe hypoinsulinemia, the *[fIrs2:cr²]:Irs1*$^{+/-}$ mice gained less weight than the *fIrs2:cr²* mice during the study period (Figure 4E). When the *[fIrs2:cr²]:Irs1*$^{+/-}$ mice were sacrificed at 6 months, relative β cell content was reduced 8-fold in comparison with the insulin-resistant but normal-sized *Irs1*$^{+/-}$ mice (Figure 4F and Table 1). Although β cells containing insulin were detected in the *[fIrs2:cr²]:Irs1*$^{+/-}$ pancreas at 6 months, the small islets were disproportionately populated by α cells (Figure 4F). The striking discrepancy between the β cell mass of *fIrs2:cr²:Irs1*$^{+/-}$mice compared with *fIrs2:cr²* mice was unexpected, as β cells retaining *fIrs2* alleles should grow in both cases; unfortunately, it was impossible to isolate intact islets from 6 month old *[fIrs2:cr²]:Irs1*$^{+/-}$ mice for genotyping.

Hypothalamic function in fIrs2:cr² mice. The *fIrs2:cr²* mice closely resemble agouti mice or mice deficient in *pro-opiomelanocortin* (*Pomc*$^{-/-}$) or *melanocortin 4 receptor* (*Mc4r*$^{-/-}$) (15), which suggests that Irs2 mediates some effects of insulin upon the melanocortin pathway in the hypothalamus. To evaluate insulin signaling, we prepared hypothalamic extracts from WT or *fIrs2:cr²* mice 15

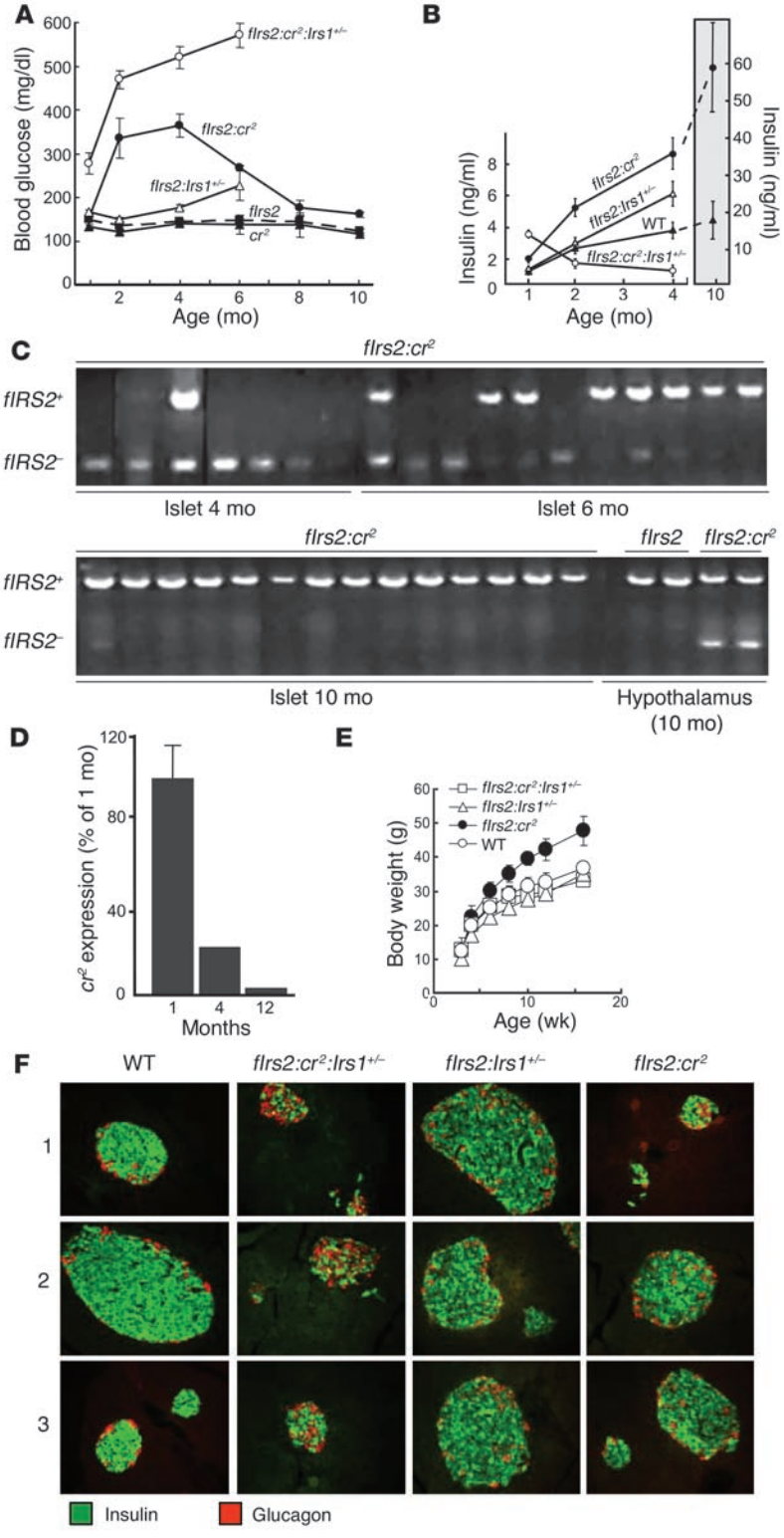

Figure 4
Pancreas β cell function in aged *flrs2:cr²* and *flrs2:cr²:lrs1*$^{+/-}$ mice. (**A**) Random-fed blood glucose levels were determined at the indicated ages. Averages ± SE were determined from at least 5 male mice per genotype. (**B**) Random insulin levels were determined in male mice of the indicated genotypes and ages. Averages ± SE were determined from at least 5 mice per genotype. (**C**) Cre-mediated recombination/deletion of *flrs2* alleles was determined by real-time PCR analysis in single islets isolated from male *flrs2:cr²* mice at the indicated ages; or determined in hypothalamus from 10-month-old *flrs2* or *flrs2:cr²* mice. (**D**) Real-time PCR analysis of *cr²* expression in isolated *flrs2:cr²* islets at the indicated ages; mRNA levels were normalized against cyclophilin expression, and the averages ± SE were determined for 2 male mice at each age. (**E**) Body weight of male littermates of the indicated genotypes that were fed regular chow and weighed weekly from postnatal day 21 until 16 weeks of age; each point represents the average ± SE of at least 6 mice. (**F**) Three representative pancreatic sections obtained from 6-month-old mice of the indicated genotypes immunostained with antibodies against insulin (green) or glucagon (red).

minutes after intravenous insulin or saline injections. Irs2 protein levels and tyrosine phosphorylation were reduced 30% in *flrs2:cr²* extracts in comparison with WT, whereas levels of signal transducer and activator of transcription 3 (Stat3) protein — measured as a control — were equal in both mice (Figure 5A). Moreover, less p85α/β was detected in Irs2 immunoprecipitates, and insulin-stimulated Akt phosphorylation was decreased in *flrs2:cr²* hypothalamic extracts (Figure 5A). These results confirmed that insulin signaling was reduced in *flrs2:cr²* hypothalamus. By comparison, leptin-stimulated Stat3 or Akt phosphorylation were not significantly changed in *flrs2:cr²* mice (data not shown).

Food intake and insulin secretion increases αMSH secretion from POMC neurons in the hypothalamus, which stimulate MC4R signaling that promotes satiety (35). Our results were consistent with characteristics of reduced MC4R signaling, including excess appetite: *Pomc1* mRNA levels — measured on Affymetrix GeneChip Mouse Expression Array 430A — were reduced almost 2-fold (90% confidence) in the hypothalamus of 16-hour–starved *flrs2:cr²* mice (Figure 5B). Other neuropeptide mRNAs — neuropeptide Y (Npy), agouti-related protein (Agrp), and cocaine and amphetamine regulated transcript (Cart) — were not changed; and the mRNA levels encoding Stat3, suppressor of cytokine signaling 3 (Socs3), and pro-protein convertase-2 — which processes αMSH — were normal (Figure 5B).

Since αMSH is a product of the POMC transcript in the arcuate nucleus, we immunostained hypothalamic sections from 8-week-old WT or *flrs2:cr²* mice with antibodies against Irs2 or αMSH (Figure 5C). The size of the hypothalamus appeared normal. In WT mice, Irs2 and αMSH were coexpressed — as indicated by the yellow staining — in many but not all of the neurons near the 3rd ventricle; however, yellow staining was absent in the *flrs2:cr²* sections, which suggested that many αMSH neurons no longer expressed Irs2. These results show that some POMC neurons in the arcuate nucleus of *flrs2:cr²* mice were uncoupled from Irs2 signaling.

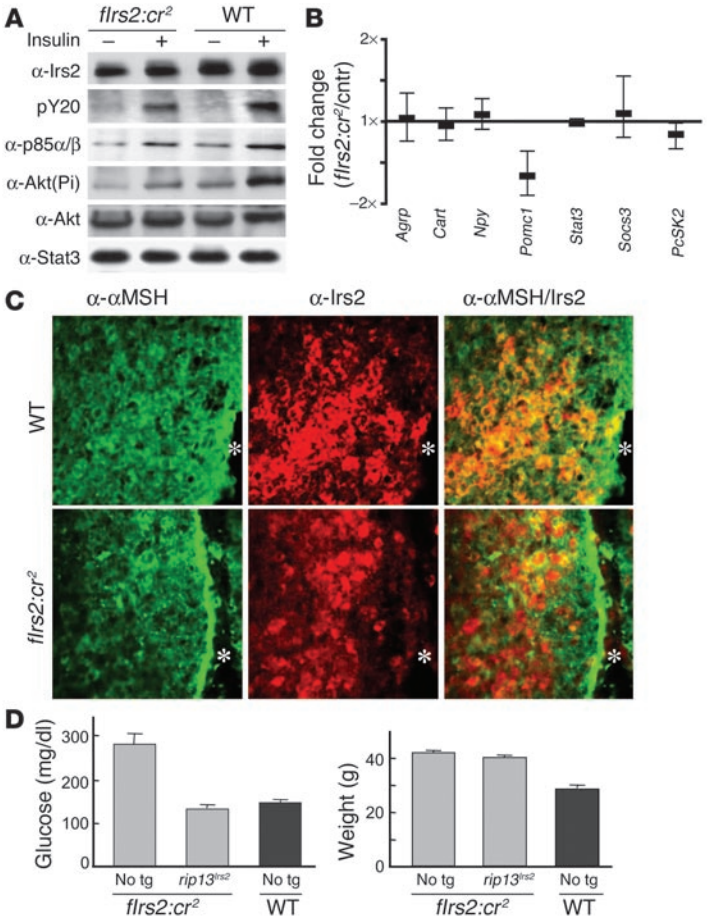

Figure 5
Analysis of hypothalamic function in the *flrs2:cr²* mice. (**A**) Immunoblots of hypothalamus lysates. After an overnight fasting, anesthetized 8-week-old mice were injected intravenously with 50 μl of saline or saline containing 5 units of insulin. Fifteen minutes later, the hypothalamus was isolated and lysed. Lysates were immunoprecipitated with anti–Irs2 antibody, resolved by SDS-PAGE, and then immunoblotted with antibodies against Irs2, phosphotyrosine (pY20), or p85. Lysates were also blotted independently with antibodies against Akt or phospho-Akt [Akt(Pi)], or Stat3. Data are representative of at least three independent experiments. (**B**) The relative expression of various mRNAs—*Npy* (1421690_s_at), *Agrp* (1419127_at), *Cart* (1422825_at) or *Pomc1* (1455858_x_at; 1433800_a_at), *Stat3* (1426587_a_at; 1426587_a_at; 1460700_at), *Socs3* (1455899_x_at; 1456212_x_at) or *PcSK2* (1448312_at; 1444147_at) was determined in hypothalamic extracts using Affymetrix GeneChip Mouse Expression Array 430A. The fold change is shown with the 90% confidence interval for expression in 3 *flrs2:cr²* mice compared with the average control values from two WT, 2 *cr²* and 2 *flrs2* mice. Where more than one probe occurs on the Genechip, the average is reported. Cntr, control. (**C**) Brain sections from WT or *flrs2:cr²* mice were immunostained with antibodies against αMSH (green) or Irs2 (red). Yellow appears in the digitally merged images where αMSH and Irs2 are coexpressed. Magnification, ×20; *3rd ventricle. (**D**) Body weight and blood glucose levels of *flrs2:cr²*, *[flrs2:cr²]:rip13^Irs2*, and WT male mice at 8 weeks; average ± SE was determined from 5 animals of each genotype. No tg, no transgene.

To confirm that weight gained by the *flrs2:cr²* mice during the first 8 weeks of life was due to dysregulated Irs2 signaling in the CNS and not β cell failure, we restored β cell function by introducing transgenic *Irs2* into the β cells of *flrs2:cr²* mice. This was accomplished through an intercross with *rip13^Irs2* mice, which express recombinant Irs2 in the β cells but not in the hypothalamus (9). Hyperglycemia did not occur in the *[flrs2:cr²]:rip13^Irs2* mice; however, the mice continued to gain excess weight (Figure 5D). Thus, partially dysregulated Irs2 signaling in the brain, rather than in β cells, appears to be responsible for hyperphagia and obesity in the *flrs2:cr²* mice.

Discussion

Our results show that partial dysregulation of Irs2 signaling in β cells and brain — including the hypothalamus — may explain the close association between obesity, peripheral insulin resistance, and β cell failure that characterizes type 2 diabetes. Whether dysregulation of IRS2 signaling contributes to type 2 diabetes and obesity in humans is unknown. However, allelic variations at the human IRS2 locus appear to be linked to obesity, glucose intolerance, and polycystic ovarian syndrome (36–38). Moreover, IRS1 and IRS2 functions are strongly inhibited by many heterologous signals, especially proinflammatory cytokines produced during acute trauma or chronic metabolic stress (5). Moreover, IRS2 expression is strongly induced by the cAMP response element binding protein (CREB), which is activated by cAMP agonists, including glucagon-like peptide 1 (GLP1) in β cells (10). Dysregulation of GLP1 signaling has been reported in type 2 diabetes, which might impair IRS2 expression in β cells and the brain (39, 40).

Male *flrs2:cr²* mice develop diabetes between 2 and 3 months of age, at least in part because β cells fail to compensate for peripheral insulin resistance. Unlike systemic *Irs2^−/−* mice that develop life-threatening diabetes earlier in life owing to complete loss of β cells, the *flrs2:cr²* mice survive with diabetes until β cell regeneration repopulates the islets with functional β cells that cure diabetes. In *flrs2:cr²* mice, the new β cells must arise from cells that never expressed Cre. The progressive decline of Cre recombinase in islets is consistent with this mechanism. Inactivation of *cr²* by hyperglycemia — as shown for the insulin-2 gene itself—might explain the progressive loss of Cre that prevented deletion of *flrs2* alleles in the new β cells (41); however, more work is need to understand the exact mechanism involved.

New β cells are thought to arise by division of β cells themselves; by differentiation of islet precursors residing in pancreatic duct epithelium; or from bone marrow (42). Direct lineage tracing in adult mice suggests that terminally differentiated β cells retain a significant proliferative capacity in vivo and are an important — and possibly the only — source of new β cells in adult mice (42). If β cells that never express Cre recombinase are the sole source of islet regeneration in the *flrs2:cr²* mouse, the regenerative capacity must be significant. Intact *flrs2* is barely detected in pooled islets at 2 months of age, which is consistent with previous reports showing that *cr²* mediates nearly complete deletion of floxed genes in β cells (32, 43, 44). At least a portion of the weak PCR signal revealing

intact *fIrs2* in these islets arises from non–β cells. Thus, β cells in *fIrs2:cr²* islets that retain Irs2 expression represent a distinct minority. Regardless of the source of regenerated β cells, IRS2 signaling must play an important role in the process.

By contrast, systemic deletion of one *Irs1* allele from *fIrs2:cr²* mice caused early-onset diabetes and impaired β cell regeneration. This result is unexpected, because Irs1 plays a limited role in islet growth (34). The absence of 1 *Irs1* allele should not inhibit regeneration if the new β cells arise by replication of a few β cells that contain intact *fIrs2*. It remains possible that Irs1-dependent precursors contributed to the expansion of β cell mass in the *fIrs2:cr²* mice. Alternatively, Irs1 signaling might sustain the function of Irs2-deficieint β cells long enough to permit the few Irs2-containing β cells an opportunity to undergo division and repopulate the islets.

Diabetes is averted by the expression of transgenic Irs2 in the *fIrs2:cr²* β cells, which suggests that strategies to promote Irs2 expression may prevent or cure type 2 diabetes. *Irs2* mRNA and Irs2 protein is strongly upregulated in β cells by cAMP → CREB signaling (10). A relevant example of this mechanism is the increased expression of IRS2 during activation of the GLP1 receptor by GLP1 itself or the long-acting homolog exendin-4 (9, 10). Improved insulin secretion, increased insulin sensitivity, and better appetite regulation reported in diabetic rodents and people treated with GLP1 or exendin-4 can be explained by increased expression of IRS2 (5, 45). Since Irs2 function is inhibited by serine phosphorylation and ubiquitin-mediated degradation that is mediated by proinflammatory cytokines (46), increased IRS2 expression together with effective management of chronic inflammation might prevent the progression of insulin resistance to diabetes.

The mild disruption of *fIrs2* by the *cr²* in the hypothalamus displays the features of dysregulated melanocortin signaling — increased appetite, lean and fat body mass, linear growth, and peripheral insulin resistance (15). Although obesity is usually thought to contribute directly to peripheral insulin resistance, lean *fIrs2:cr²* mice were also relatively insulin resistant, hyperinsulinemic, and glucose intolerant compared with the control mice. The results from the hyperinsulinemic clamp suggest that the insulin resistance in the *fIrs2:cr²* mice resides in extra hepatic tissues — most likely the skeletal muscle — as hepatic glucose output is regulated normally by insulin, whereas glucose disposal is impaired. Previous work shows that dysregulated melanocortin signaling causes peripheral insulin resistance even before obesity develops, possibly because activation of MC4Rs in the paraventricular nucleus promotes peripheral insulin action (47, 48). The reduced levels of Pomc1 mRNA in *fIrs2:cr²* hypothalamus and the loss of Irs2 from neurons that express αMSH reveal a potential mechanism for these effects. Thus, dysregulated Irs2 signaling in the brain, especially the hypothalamus, could contribute to central and peripheral insulin resistance that predisposes individuals to obesity and diabetes (25).

The deletion of floxed insulin or Igf1 receptors by *cr²* expression does not alter food intake or body weight (43, 49). If more careful analysis reveals the deletion of these receptor genes in the hypothalamus — as reported here for *fIrs2* and elsewhere for floxed *Stat3* (32) — then loss of insulin or Igf1 receptor signaling might not promote obesity. This potential result would be similar to that obtained using the phenotype of neuron-specific insulin receptor KO (NIRKO) mice; only when placed on a diet containing 60% fat do NIRKO mice develop obesity.

Our work shows that Irs2 signaling is important for β cell growth, function, and survival. Moreover, our experiments show that β cell regeneration in middle age can cure diabetes in mice and that Irs2 signaling provides a significant advantage for this regeneration. Now we must determine whether the new β cells arise from the division of a few preexisting β cells that escaped *fIrs2* deletion or from non–β cell precursors that never express Cre recombinase when they differentiate at middle age. Independent of the mechanism, strategies to enhance the Irs2 branch of the insulin/IGF-signaling pathway in β cells and hypothalamus could be a rational approach to prevent obesity and diabetes.

Methods

Targeting vector and generation of mice. All methods discussed in this section involving animals have been approved by the Institutional Animal Care and Use Committee (IACUC) of Children's Hospital Boston, and by the Harvard School of Public Health review board. *Irs2* genomic sequence was isolated from a 129 mouse genomic library as previously described (6). Two fragments of *Irs2* gene were cloned into a pPNT backbone vector that contained a neomycin selection cassette flanked by LoxP sites (Figure 1A). A 2.3-kb 5′ NheI/MscI fragment was inserted in front of the neo cassette, and an 8-kb MscI/SalI fragment — including a 200-bp 5′-untranslated region, 4-kb full-length coding sequence and the 3.8-kb 3′ region — was cloned from the neo cassette. The latter sequence contains the third LoxP site located 60-bp downstream from the stop codon. The linearized targeting vector was transfected into male R1 embryonic stem cells derived from 129 mouse strain (51). Double selection was performed with G418 and ganciclovir, and drug-resistant clones were screened for homologous recombination by Southern blotting. Recombinants were subject to transfection by a *Cre*-containing plasmid, and clones maintaining *fIrs2* but losing the neo cassette were selected by Southern analysis and injected into blastocysts from C57BL/6 mice. Chimeric male pups were bred with C57BL/6 females to confirm germ-line transmission.

cr² mice were purchased from The Jackson Laboratory and maintained in a heterozygous state. Generation of Irs1 KO mice and rip13^{Irs2} transgenic mice was as previously described (6, 9). To generate *fIrs2:cr²* mice (mice homozygous for the *fIrs2* allele and carrying *cr²* transgene), we bred heterozygous *fIrs2* with *cr²* first, and then mice double heterozygous for *fIrs2* and *cr²* were mated with *fIrs2* heterozygous mice to obtain *fIrs2:cr²* and control mice (homozygous for the *fIrs2* allele, *cr²* transgenic, and WT). To generate *fIrs2:cr²:Irs1*$^{+/-}$ and *fIrs2:cr²:rip13*^{Irs2} mice, *fIrs2:cr²* females were bred with *fIrs2:Irs1*$^{+/-}$ and *fIrs2:rip13*^{Irs2} males, respectively. All mice were maintained on a mixed C57BL/6 × 129Sv genetic background, housed in a pathogen-free environment in a 12-hour light/dark cycle facility, and fed a normal (9%) or low-fat (5%) diet (Research Diet). Routine genotyping was performed on tail DNA by PCR. Primers for *fIrs2* allele were 5′-ACTTGAAGGAAGCCACAGTCG and 3′-GTCCACTTTCCTGACAAGC. They flanked the last LoxP site and amplified a 200-bp product in WT allele and a 240-bp product in *fIrs2* allele. Genotyping for *Irs1*, *rip13*^{Irs2}, and *cr²* mice has been described (6, 9, 43).

Assessment of recombination. Mice were anesthetized with sodium amobarbital (100 mg kg^{-1}). Islets were isolated by intraductal collagenase digestion (13). Various tissues were collected for genomic DNA extraction. Recombination was assessed by PCR analysis using two 5′ and one 3′ primers. The first 5′ primer, TCCGATCATATTCAATAACCCTTA, which included part of the first LoxP sequence, paired with the 3′-primer, TACACTGAGACAGAAGGTTAGG, which was located downstream of the last LoxP site, to give rise to a 250-bp recombined product. The other 5′ primer, ACGTCGTCGCCACAGTTCAGAG, in the coding region of *Irs2*, paired with the same 3′ primer to amplify a 750-bp un-recombined *fIrs2* product.

Metabolic analysis. Body weight was measured weekly beginning on postnatal day 21. Food intake during 24 hours was determined using the Comprehensive Lab Animal Monitoring System (Columbus Instru-

ments). Lean and fat body mass were determined by dual-energy x-ray absorptiometry (52). Carcasses were digested by alcoholic potassium hydroxide hydrolysis at 60°C overnight, and body lipid was determined as described previously (53).

Glucose and insulin levels and the various tolerance tests were performed upon fasted mice (16-hour overnight fast) or random-fed mice (test conducted in the morning between 9:00 and 11:00 without an overnight fast). Glucose levels were measured in mouse-tail blood using a Glucometer Elite (Bayer), and glucose tolerance tests were performed on mice after a 16-hour overnight fast (6). Blood insulin and leptin levels were determined from tail bleeds using a Rat Insulin ELISA kit and Mouse Leptin ELISA kit (Crystal Chem Inc.) (9).

Euglycemic hyperinsulinemic clamp. Euglycemic hyperinsulinemic clamp was performed on fasted conscious mice as previously described (54). [3-^{3}H] glucose (NEN) was continuously infused during a 4-hour period at the rate of 0.05 μCi/min. Basal hepatic glucose output was measured in blood collected at 100 and 120 minutes after initiation of the [3-^{3}H] glucose infusion. Then a primed continuous infusion of human regular insulin (Humulin; Eli Lilly and Co.) was initiated at a rate of 20 pmol × kg^{-1} × min^{-1} to raise plasma insulin concentration to approximately 1100 pM. Glucose (20%) was infused at variable rates as needed to clamp glucose levels at about 6 mM. While blood glucose levels were steady between 200 and 240 minutes, the rate of glucose production was determining by measuring every 10 minutes the blood levels of [3-^{3}H] glucose and ^3H_2O. Clamped hepatic glucose output was calculated by subtracting glucose infusion rates from the rates of glucose appearance. Whole-body glucose disposal was expressed in terms of mg of glucose per kg of body weight per minute required to maintain euglycemia during hyperinsulinemia (54).

mRNA quantitation by real-time PCR analysis. Total RNA was extracted from isolated, hand-picked islets using RNAqueous-4PCR kit (Ambion Inc.), and reverse transcribed using RETROscript kit (Ambion Inc.). Real-time PCR was performed on iCycler (Bio-Rad Laboratories). Primers and fluorescence-labeled probes for *Hnf4α* were 5′: ACGTGCTGCTCCTAGGCAAT, 3′: TCGAGGATGCGGATGGA, probe: CACACGGCTCATCTCCGCTAGCTCTG; for *Hnf3β* 5′: GAACTCCATCCGCCACTCTCT, 3′: GCCCTTGCCAGGCTTGT, probe: TCAACGACTGCTTTCTCAAGGTGCCC; for *Pdx1*, 5′: AGGAAAACAAGAGGACCCGTACT, 3′: CGGGAGATGTATTTGTTAAATAAGAATTC, probe: CCTACACCCGGGCGCAGCTG; for *Glut2*, 5′: TCTTCACGGATGCCAATTACC, 3′: AGAACTGCTGGGCCATGTG, probe: AGCCCATCCTCGTGGCGCTG; for *cr*^{2}, 5′: TGGCCTGGTCTGGACACA, 3′: CCAGGTTACGGATATAGTTCATGACA, probe: TGTCCGGTATTGAAACTCCAGCGCG; for *Irs2*, 5′: GCGGCCTCATCTTCTTCACT, 3′: AACTGAAGTCCAGGTTCATATAGTCAGA, probe: CGACAGCCGGCAGCGCTCTC; for *cyclophilin*, 5′: CAGACGCCACTGTCGCTTT, 3′: TGTCTTTGGAACTTTGTCTGCAA, probe: CCTACACCCGGGCGCAGCTG. The expression of *cyclophilin* was used to normalize RNA content. Each reaction was carried out in triplicate.

Immunoprecipitation and Western blotting. After an overnight (15- to 17-hour) fast, mice were anesthetized before an insulin (5 units regular human insulin) or saline injection into the inferior vena cava. Fifteen minutes after injection, hypothalamus was removed and homogenized. Clarified supernatants containing 400 μg of total protein were immunoprecipitated with anti–Irs2 antibody as described (6). Immunoblots were probed with anti–Irs2 antibody to reveal Irs2 expression levels, with anti–phosphotyrosine antibody (pY20; Transduction Laboratories) to reveal insulin-stimulated Irs2 phosphorylation, and with anti–p85α/β antibody to reveal PI3K activation in an indirect manner. To assess insulin-stimulated Akt activation, 50 μg of supernatants was separated by SDS-PAGE and transferred to nitrocellulose. Membranes were probed with phospho-specific anti–Akt antibody (Cell Signaling Technology). The same membranes were stripped and re-probed with anti–Akt antibody (Cell Signaling Technology) to reveal Akt expression levels. Membranes were probed with anti–Stat3 antibody (Cell Signaling Technology) to serve as a protein loading control. The antibodies were detected by enhanced chemiluminescence (Calbiochem) and quantified using ImageQuant software (Amersham Biosciences).

Immunohistochemistry and morphometric analysis. Pancreata were removed from mice, cleared of fat and lymph nodes, fixed overnight in 4% paraformaldehyde, and embedded in paraffin. Sections (5 μm in thickness) were stained with anti–insulin antibody (Jackson ImmunoResearch Laboratories Inc.). β Cell area was presented as percentage of the total surveyed pancreatic area occupied by β cells and determined by point-counting morphometry as previously described (6). Briefly, sections were viewed using a Zeiss Axiovert S100 TV (Carl Zeiss) microscope at a magnification of ×10. The islet cross-sectional area and total pancreatic area were measured using Openlab Image analysis software (version 3.14; Improvision). β Cell mass was calculated by multiplying β cell area by pancreatic weight. β Cell size was determined by dividing β cell area by β cell number. β Cell proliferation was determined by BrdU incorporation (100 μg/g body weight; Roche Molecular Biochemicals) was injected intraperitoneally 6 hours before pancreas was collected. Double immunostaining for insulin and BrdU (Roche Molecular Biochemicals) was performed on pancreas sections. To distinguish between large (>10 β cells) and small (<10 β cells) islets, 1 entire section of pancreas immunostained by insulin — from 3 or 4 mice as indicated — was examined. For immunostaining of brain sections, mice were perfused with 10% formalin, and then whole brain was sliced with Microtome (American Optical Company). Thirty-μm-thick sections were stained with antibodies against Irs2 (UBI), Cre (Covance), or αMSH (Chemicon). Grayscale images were normalized using ImageJ software, aligned using the Turbo Registration plug-in to ImageJ, then recolored as shown in the figures (55).

Microarray analysis. After an overnight fast, the hypothalamus was collected from 2 WT, 2 *flrs2*, 2 *cr*^{2} mice, and 3 *flrs2:cr*^{2} 8-week-old mice. Total RNA was extracted and purified from each sample using RNAqueous-4PCR Kit (Ambion Inc.). cDNA synthesis and in vitro transcription was carried out using SuperScript Choice System (Invitrogen) and MEGAscript T7 Kit (Ambion Inc.) according to the manufacturers' instructions. Labeled probes were prepared by in vitro transcription using second-cycle cDNA synthesis products, and the samples were hybridized to Affymetrix GeneChip Mouse Expression Array 430A in a GeneChip Fluidics Station 400 and scanned with a Hewlett-Packard GeneArray Scanner (56). The data files (dat format) were normalized to the median array using dCHIP software (version 1.31), and the expression levels were calculated using the perfect match–only model (57). All of the reported genes were flagged as present by both Affymetrix GeneChip (version 5.0) and dCHIP. The fold change and the 90% confidence interval were calculated for average *flrs2:cr*^{2} samples (n = 3) against the average control samples (n = 6).

Acknowledgments

This work was supported by NIH grant DK55236. X. Lin was a Juvenile Diabetes Foundation (JDF) postdoctoral fellow while this work was conducted.

Received for publication May 20, 2004, and accepted in revised form July 20, 2004.

Address correspondence to: Morris F. White, Howard Hughes Medical Institute Children's Hospital, Division of Endocrinology, Harvard Medical School, Karp Research Building, Room 04210, 300 Longwood Avenue, Boston, Massachusetts 02115, USA. Phone: (617) 919-2846; E-mail: morris.white@childrens.harvard.edu.

1. Zimmet, P., Alberti, K.G., and Shaw, J. 2001. Global and societal implications of the diabetes epidemic. *Nature.* **414**:782–787.
2. Diamond, J. 2003. The double puzzle of diabetes. *Nature.* **423**:599–602.
3. DeFronzo, R.A. 1988. Lilly lecture 1987. The triumvirate: beta-cell, muscle, liver. A collusion responsible for NIDDM [review]. *Diabetes.* **37**:667–687.
4. Shulman, G.I. 2000. Cellular mechanisms of insulin resistance. *J. Clin. Invest.* **106**:171–176.
5. White, M.F. 2003. Insulin signaling in health and disease. *Science.* **302**:1710–1711.
6. Withers, D.J., et al. 1998. Disruption of IRS-2 causes type 2 diabetes in mice. *Nature.* **391**:900–904.
7. Kubota, N., et al. 2000. Disruption of insulin receptor substrate 2 causes type 2 diabetes because of liver insulin resistance and lack of compensatory beta-cell hyperplasia. *Diabetes.* **49**:1880–1889.
8. Previs, S.F., Withers, D.J., Ren, J.M., White, M.F., and Shulman, G.I. 2000. Contrasting effects of IRS-1 vs IRS-2 gene disruption on carbohydrate and lipid metabolism in vivo. *J. Biol. Chem.* **275**:38990–38994.
9. Hennige, A.M., et al. 2003. Upregulation of insulin receptor substrate-2 in pancreatic β cells prevents diabetes. *J. Clin. Invest.* **112**:1521–1532. doi:10.1172/JCI200318581.
10. Jhala, U.S., et al. 2003. cAMP promotes pancreatic beta-cell survival via CREB-mediated induction of IRS2. *Genes Dev.* **17**:1575–1580.
11. Kushner, J.A., et al. 2004. Islet-sparing effects of protein tyrosine phosphatase-1b deficiency delays onset of diabetes in IRS2 knockout mice. *Diabetes.* **53**:61–66.
12. Kitamura, T., et al. 2002. The forkhead transcription factor *Foxo1* links insulin signaling to *Pdx1* regulation of pancreatic β cell growth. *J. Clin. Invest.* **110**:1839–1847. doi:10.1172/JCI200216857.
13. Kushner, J.A., et al. 2002. Pdx1 restores β cell function in Irs2 knockout mice. *J. Clin. Invest.* **109**:1193–1201. doi:10.1172/JCI200214439.
14. Suzuki, R., et al. 2003. Pdx1 expression in Irs2-deficient mouse beta-cells is regulated in a strain-dependent manner. *J. Biol. Chem.* **278**:43691–43698.
15. Butler, A.A., and Cone, R.D. 2003. Knockout studies defining different roles for melanocortin receptors in energy homeostasis. *Ann. N. Y. Acad. Sci.* **994**:240–245.
16. Farooqi, I.S., et al. 2003. Clinical spectrum of obesity and mutations in the melanocortin 4 receptor gene. *N. Engl. J. Med.* **348**:1085–1095.
17. Schwartz, M.W., et al. 2000. Central nervous system control of food intake. *Nature.* **404**:661–671.
18. Qi, Y., et al. 2004. Adiponectin acts in the brain to decrease body weight. *Nat. Med.* **10**:524–529.
19. Myers, M.G., Jr. 2004. Leptin receptor signaling and the regulation of mammalian physiology. *Recent Prog. Horm. Res.* **59**:287–304.
20. Woods, S.C., Lotter, E.C., McKay, L.D., and Porte, D., Jr. 1979. Chronic intracerebroventricular infusion of insulin reduces food intake and body weight of baboons. *Nature.* **282**:503–505.
21. Schwartz, M., Figlewicz, D.P., Baskin, D.G., Woods, S.C., and Porte, D. 1992. Insulin in the brain: A hormonal regulator of energy balance. *Endocr. Rev.* **13**:387–414.
22. Schwartz, M.W., Baskin, D.G., Kaiyala, K.J., and Woods, S.C. 1999. Model of the regulation of energy balance and adiposity by the central nervous system. *Am. J. Clin. Nutr.* **69**:584–596.
23. Bruning, J.C., et al. 2000. Role of brain insulin receptor in control of body weight and reproduction. *Science.* **289**:2122–2125.
24. Huszar, D., et al. 1997. Targeted disruption of the melanocortin-4 receptor results in obesity in mice. *Cell.* **88**:131–141.
25. Obici, S., et al. 2001. Central melanocortin receptors regulate insulin action. *J. Clin. Invest.* **108**:1079–1085. doi:10.1172/JCI200112954.
26. Challis, B.G., et al. 2002. A missense mutation disrupting a dibasic prohormone processing site in pro-opiomelanocortin (POMC) increases susceptibility to early-onset obesity through a novel molecular mechanism. *Hum. Mol. Genet.* **11**:1997–2004.
27. Yamauchi, T., et al. 2003. Cloning of adiponectin receptors that mediate antidiabetic metabolic effects. *Nature.* **423**:762–769.
28. Combs, T.P., et al. 2003. Sexual differentiation, pregnancy, calorie restriction, and aging affect the adipocyte-specific secretory protein adiponectin. *Diabetes.* **52**:268–276.
29. Spranger, J., et al. 2003. Adiponectin and protection against type 2 diabetes mellitus. *Lancet.* **361**:226–228.
30. Burks, D.J., et al. 2000. IRS-2 pathways integrate female reproduction and energy homeostasis. *Nature.* **407**:377–382.
31. Gannon, M., Shiota, C., Postic, C., Wright, C.V., and Magnuson, M. 2000. Analysis of the Cre-mediated recombination driven by rat insulin promoter in embryonic and adult mouse pancreas. *Genesis.* **26**:139–142.
32. Cui, Y., et al. 2004. Essential role of STAT3 in body weight and glucose homeostasis. *Mol. Cell. Biol.* **24**:258–269.
33. Schubert, M., et al. 2003. Insulin receptor substrate-2 deficiency impairs brain growth and promotes tau phosphorylation. *J. Neurosci.* **23**:7084–7092.
34. Withers, D.J., et al. 1999. Irs-2 coordinates Igf-1 receptor-mediated beta-cell development and peripheral insulin signalling. *Nat. Genet.* **23**:32–40.
35. Schwartz, M.W. 2001. Progress in the search for neuronal mechanisms coupling type 2 diabetes to obesity. *J. Clin. Invest.* **108**:963–964. doi:10.1172/JCI200114127.
36. Lautier, C., et al. 2003. Complex haplotypes of IRS2 gene are associated with severe obesity and reveal heterogeneity in the effect of Gly1057Asp mutation. *Hum. Genet.* **113**:34–43.
37. Ehrmann, D.A., Tang, X., Yoshiuchi, I., Cox, N.J., and Bell, G.I. 2002. Relationship of insulin receptor substrate-1 and -2 genotypes to phenotypic features of polycystic ovary syndrome. *J. Clin. Endocrinol. Metab.* **87**:4297–4300.
38. Stefan, N., et al. 2004. The Gly1057Asp polymorphism in IRS-2 interacts with obesity to affect beta cell function. *Diabetologia.* **47**:759–761.
39. Brubaker, P.L., and Drucker, D.J. 2004. Glucagon-like peptides regulate cell proliferation and apoptosis in the pancreas, gut and central nervous system. *Endocrinology.* **145**:2653–2659.
40. During, M.J., et al. 2003. Glucagon-like peptide-1 receptor is involved in learning and neuroprotection. *Nat. Med.* **9**:1173–1179.
41. Ling, Z., Heimberg, H., Foriers, A., Schuit, F., and Pipeleers, D. 1998. Differential expression of rat insulin I and II messenger ribonucleic acid after prolonged exposure of islet beta-cells to elevated glucose levels. *Endocrinology.* **139**:491–495.
42. Dor, Y., Brown, J., Martinez, O.I., and Melton, D.A. 2004. Adult pancreatic beta-cells are formed by self-duplication rather than stem-cell differentiation. *Nature.* **429**:41–46.
43. Kulkarni, R.N., et al. 1999. Tissue-specific knockout of the insulin receptor in pancreatic β cells creates an insulin secretory defect similar to that in type 2 diabetes. *Cell.* **96**:329–339.
44. Postic, C., et al. 1999. Dual roles for glucokinase in glucose homeostasis as determined by liver and pancreatc beta cell-specific gene knock-outs using Cre recombinase. *J. Biol. Chem.* **274**:305–315.
45. Zander, M., Madsbad, S., Madsen, J.L., and Holst, J.J. 2002. Effect of 6-week course of glucagon-like peptide 1 on glycaemic control, insulin sensitivity, and beta-cell function in type 2 diabetes: a parallel-group study. *Lancet.* **359**:824–830.
46. Rui, L., Yuan, M., Frantz, D., Shoelson, S., and White, M.F. 2002. SOCS-1 and SOCS-3 block insulin signaling by ubiquitin-mediated degradation of IRS1 and IRS2. *J. Biol. Chem.* **277**:42394–42398.
47. Shimomura, I., et al. 2000. Decreased IRS-2 and increased SREBP-1c lead to mixed insulin resistance and sensitivity in livers of lipodystrophic and ob/ob mice. *Mol. Cell.* **6**:77–86.
48. Obici, S., Feng, Z., Karkanias, G., Baskin, D.G., and Rossetti, L. 2002. Decreasing hypothalamic insulin receptors causes hyperphagia and insulin resistance in rats. *Nat. Neurosci.* **5**:566–572.
49. Kulkarni, R.N., et al. 2002. beta-cell-specific deletion of the Igf1 receptor leads to hyperinsulinemia and glucose intolerance but does not alter beta-cell mass. *Nat. Genet.* **31**:111–115.
50. Niswender, K.D., et al. 2003. Insulin activation of phosphatidylinositol 3-kinase in the hypothalamic arcuate nucleus: a key mediator of insulin-induced anorexia. *Diabetes.* **52**:227–231.
51. Wood, S.A., Allen, N.D., Rossant, J., Auerbach, A., and Nagy, A. 1993. Non-injection methods for the production of embryonic stem cell-embryo chimaeras. *Nature.* **365**:87–89.
52. Nagy, T.R., and Clair, A.L. 2000. Precision and accuracy of dual-energy X-ray absorptiometry for determining in vivo body composition of mice. *Obes. Res.* **8**:392–398.
53. Fredrich, R.C., et al. 1995. Leptin levels reflect body lipid content in mice: evidence for diet-induced resistance to leptin action. *Nat. Med.* **1**:1311–1314.
54. Kim, J.K., et al. 2001. Tissue-specific overexpression of lipoprotein lipase causes tissue-specific insulin resistance. *Proc. Natl. Acad. Sci. U. S. A.* **98**:7522–7527.
55. Thevenaz, P., Ruttimann, U.E., and Unser, M. 1998. A pyramid approach to subpixel registration based on intentisy. *IEEE Trans. Image Process.* **7**:27–41.
56. MIT Biopolymers Laboratory. http://web.mit.edu/biopolymers/www/.
57. Li, C., and Wong, W.H. 2001. Model-based analysis of oligonucleotide arrays: expression index computation and outlier detection. *Proc. Natl. Acad. Sci. U. S. A.* **98**:31–36.